COMPUTATIONAL METHODS IN APPLIED MATHEMATICS, Vol. 10 (2010), No. 1, pp. 49–68

A POSTERIORI ERROR ESTIMATORS BASED ON EQUILIBRATED FLUXES

S. COCHEZ-DHONDT[1] AND S. NICAISE[1]

Abstract — We consider the conforming of finite element approximations of reaction-diffusion problems. We propose new a posteriori error estimators based on $H(\mathrm{div})$-conforming finite elements and equilibrated fluxes. It is shown that these estimators give rise to an upper bound where the constant is one in front of the indicator, up to higher order terms. Lower bounds can also be established with constants depending on the shape regularity of the mesh and the local variation of the coefficients. We further analyze the convergence of an adaptive algorithm. The reliability and efficiency of the proposed estimators are confirmed by various numerical tests.

2000 Mathematics Subject Classification: 65N30, 65N15, 65N50.

Keywords: equilibrated fluxes, reaction-diffusion problems, a posteriori error estimates.

1. Introduction

Among other methods, the finite element method is widely used for the numerical approximation of partial differential equations (see, e.g., [3–5,7,14]). In many engineering applications, adaptive techniques based on a posteriori error estimators have become an indispensable tool for obtaining reliable results. Nowadays there exists a vast amount of literature on locally defined a posteriori error estimators for problems in structural mechanics or electromagnetism. We refer to the monographs [1, 2, 15, 23] for a good overview on this topic. In general, local upper and lower bounds are established in order to guarantee the reliability and the efficiency of the proposed estimator. Most of the existing approaches involve constants depending on the shape regularity of the elements and/or of the jumps in the coefficients; but these dependencies are often not given. Only a small number of approaches give rise to estimates with explicit constants (see, e.g., [1, 3, 11, 12, 19, 22]). Here we use an approach based on equilibrated fluxes and $H(\mathrm{div})$-conforming elements. Similar ideas can be found, e.g., in [3,12,22]. For an overview on equilibration techniques, we refer to [1,11]. For reaction-diffusion problems, in contrast to [3], we first define on the edges an equilibrated flux and then a $H(\mathrm{div})$-conforming element being locally conservative by construction. In [3], the authors consider a Laplace equation and directly compute suitable conforming elements by solving local Neumann problems. In both cases, the error estimator is locally defined and yields, up to higher order terms, an upper bound with constant one in front of the indicator. We note that our error estimators are made for partial differential equations with zero order terms, and the upper bound one is still valid in this more general situation. Special

[1] *Univ Lille Nord de France*, F-59000 Lille, France; UVHC, LAMAV, F-59313 Valenciennes, France (corresponding address); CNRS, FR 2956, F-59655 Villeneuve d'Ascq, France. E-mail: Sarah.Cochez,Serge.Nicaise@univ-valenciennes.fr

care is required by the lower order terms. Furthermore, lower bounds are proved, where we trace the dependence of the constants with respect to the variation of the coefficients for all proposed estimators.

Finally, for elliptic problems, there exists a large amount of papers on the convergence of adaptive finite element methods, let us quote [6, 9, 13, 16–18]. Inspired by those papers, we analyze the convergence of an adaptive algorithm based on our estimator, on a bulk criterion, and on the refinement procedure REFINE of Morin, Nochetto and Siebert [13, 16, 17].

The outline of the paper is as follows. We recall, in Section 2, the scalar reaction-diffusion problem and its numerical approximation. Section 3 is devoted to the introduction of the locally defined error estimators based on Raviart — Thomas or Brezzi — Douglas — Marini (BDM) elements and to the proofs of the upper and lower bounds. The upper bound directly follows from the construction of the estimators, while the proof of the lower bound relies on suitable norm equivalences and some properties of the equilibrated fluxes. The convergence of an adaptive algorithm is given in section 4 and is based on the upper bound proved before and on a reduction of the error proved like the lower bound. Finally, some numerical tests confirming the reliability and efficiency of our error estimators are presented.

2. The two-dimensional reaction — diffusion equation

Let Ω be a bounded domain of $\mathbb{R}^2$ and Γ its polygonal boundary. We consider the following elliptic second order boundary value problem with homogeneous mixed boundary conditions:

$$\begin{aligned} -\mathrm{div}(a\,\nabla u) + u &= f \quad \text{in } \Omega, \\ u &= 0 \quad \text{on } \Gamma_D, \\ a\nabla u \cdot n &= 0 \quad \text{on } \Gamma_N, \end{aligned} \tag{2.1}$$

where $\Gamma = \bar{\Gamma}_D \cup \bar{\Gamma}_N$ and $\Gamma_D \cap \Gamma_N = \varnothing$.

In the sequel, we suppose that a is piecewise constant, namely we assume that there exists a partition $\mathcal{P}$ of Ω into a finite set of Lipschitz polygonal domains $\Omega_1, \ldots, \Omega_J$ such that, on each Ω_j, $a = a_j$ where a_j is a positive constant. For simplicity of notation, we assume that Γ_D has a nonvanishing measure. The variational formulation of (2.1) involves the bilinear form

$$B(u,v) = \int_\Omega (a\nabla u \cdot \nabla v + uv)\,.$$

Given $f \in L^2(\Omega)$, the weak formulation consists in finding $u \in H^1_D(\Omega) := \{u \in H^1(\Omega) : u = 0 \text{ on } \Gamma_D\}$ such that

$$B(u,v) = (f,v) = \int_\Omega fv, \quad \forall v \in H^1_D(\Omega). \tag{2.2}$$

We consider a triangulation $\mathcal{T}_h$ made of triangles T whose edges are denoted by e and assume that this triangulation is shape-regular, i.e., for any element T, the ratio h_T/ρ_T is bounded by a constant $\sigma > 0$ independent of $T \in \mathcal{T}_h$ and of the mesh-size $h = \max_{T\in\mathcal{T}_h} h_T$, where h_T is the diameter of T and ρ_T is the diameter of its largest inscribed ball. We further assume that $\mathcal{T}_h$ is conforming with the partition $\mathcal{P}$ of Ω, i.e., any $T \in \mathcal{T}_h$ is included in one and only one Ω_i. With each edge e of the triangulation, we associate a fixed unit normal vector n_e, and n_T stands for the outer unit normal vector of T. For boundary edges

$e \subset \partial\Omega \cap \partial T$, we set $n_e = n_T$. $\mathcal{E}_h$ represents the set of edges of the triangulation, and we assume that the Dirichlet boundary can be written as a union of edges. In the sequel, a_T denotes the value of the piecewise constant coefficient a restricted to the element T.

In the following, the L^2-norm on a subdomain D will be denoted by $\|\cdot\|_D$; the index will be dropped if $D = \Omega$. We use $\|\cdot\|_{s,D}$ and $|\cdot|_{s,D}$ to denote the standard norm and semi-norm on $H^s(D)$ $(s \geqslant 0)$, respectively. The energy norm is defined by $|||v|||^2 = B(v,v)$, for any $v \in H^1(\Omega)$. Finally, the notation $r \lesssim s$ and $r \sim s$ means the existence of positive constants C_1 and C_2, which are independent of the mesh size, of the coefficients of the partial differential equation, and of the quantities r and s such that $r \leqslant C_2 s$ and $C_1 s \leqslant r \leqslant C_2 s$, respectively.

Problem (2.2) is approximated by a conforming finite element subspace of $H^1_D(\Omega)$:

$$X_h = \left\{ v_h \in H^1_D(\Omega) \mid v_{h|T} \in \mathbb{P}_1(T), \quad T \in \mathcal{T}_h \right\}$$

and the finite element solution $u_h \in X_h$ satisfies the discretized problem

$$B(u_h, v_h) = (f, v_h), \quad \forall v_h \in X_h. \tag{2.3}$$

For further purposes we introduce a set of fluxes $\{g_e \in \mathbb{P}_1(e) \mid e \in \mathcal{E}_h\}$ that satisfy the local variational problem

$$B_T(u_h, v_h) = \int_T f\, v_h + \int_{\partial T} g_T v_h, \quad \forall v_h \in \mathbb{P}_1(T), \quad T \in \mathcal{T}_h, \tag{2.4}$$

where $B_T(\cdot,\cdot)$ represents the local contribution of the bilinear form $B(\cdot,\cdot)$ on the element T and $g_{T|e} = g_e\ n_e \cdot n_T$. The existence of such fluxes is guaranteed and g_e can be locally constructed in terms of its moments and the solution of a local vertex based system (see, e.g., [1, 12]). We note that g_e approximates the flux of the exact solution and thus we set $g_e = 0$ if $e \subset \Gamma_N$.

3. Upper and lower bounds for the error estimator

Error estimators can be constructed in many different ways, for example, by using residual type error estimators which measure locally the jump of the discrete flux. A different method based on equilibrated fluxes consists in solving local Neumann boundary value problems [1]. Here, introducing the flux as an auxiliary variable, we locally define an error estimator based on the $H(\mathrm{div})$-conforming approximation of this variable. This method avoids solving the above-mentioned supplementary local subproblems. Indeed, in many applications the flux $j = a\nabla u$ is an important quantity, and introducing this auxiliary variable, we transform the original problem (2.2) into a first order system. Its weak formulation gives rise to the following saddle point problem: Find $(j,u) \in H_N(\mathrm{div},\Omega) \times L^2(\Omega)$ such that

$$\int_\Omega a^{-1} j\ \tau + \int_\Omega \mathrm{div}\tau\ u = 0, \quad \forall \tau \in H_N(\mathrm{div},\Omega), \tag{3.1}$$

$$\int_\Omega \mathrm{div} j\ w - \int_\Omega u\ w = -\int_\Omega f\ w, \quad \forall w \in L^2(\Omega), \tag{3.2}$$

the natural space for the flux being

$$H_N(\mathrm{div},\Omega) = \left\{ q \in [L^2(\Omega)]^2 \mid \mathrm{div} q \in L^2(\Omega) \ \text{ and } \ q \cdot n = 0 \ \text{ on } \ \Gamma_N \right\}.$$

Therefore, the discrete flux approximation j_h will be searched in an $H(\mathrm{div})$-conforming space based on standard mixed finite elements. Hence different error estimators can be defined in terms of different mixed finite element spaces such as, e.g., Raviart — Thomas finite elements or BDM elements. Here, for simplicity we only consider low order finite elements but all ideas can easily be generalized to higher order finite elements. We consider three different cases and introduce the inf-sup stable pairs (V_h^i, W_h^i), $i = 1, 2, 3$ by

$$V_h^i = \left\{ v_h \in H_N(\mathrm{div},\Omega) \mid v_{h|T} \in V^i(T), \ \ T \in \mathfrak{T}_h \right\},$$

$$W_h^i = \left\{ w_h \in L^2(\Omega) \mid w_{h|T} \in W^i(T), \ \ T \in \mathfrak{T}_h \right\},$$

where $V^1(T) = RT_0(T)$, $V^2(T) = BDM_1(T)$, $V^3(T) = RT_1(T)$ and $W^1(T) = W^2(T) = \mathbb{P}_0(T)$, $W^3(T) = \mathbb{P}_1(T)$. Here, we use the definition of the local Raviart — Thomas and BDM elements $RT_l(T) = (\mathbb{P}_l(T))^2 + \mathbb{P}_l(T)\boldsymbol{x}$, $l = 0, 1$ and $BDM_1 = (\mathbb{P}_1(T))^2$. We note that $V^1(T) \subset V^2(T) \subset V^3(T)$. Then it is well known (see, e.g., [5]) that $\mathrm{div} V_h^i = W_h^i$. We denote by Π_h^i the L^2-projection onto W_h^i. Now we introduce a locally defined flux $j_h^i \in V_h^i$. It is uniquely defined in terms of its degrees of freedom and can be determined with the help of g_e and u_h:

$i = 1$: for all edges $e \in \mathcal{E}_h$

$$\int_e j_h^1 \cdot n_e = \int_e g_e,$$

$i = 2$: for all edges $e \in \mathcal{E}_h$

$$\int_e j_h^2 \cdot n_e q = \int_e g_e q, \quad \forall q \in \mathbb{P}_1(e),$$

$i = 3$ for all edges $e \in \mathcal{E}_h$ and all elements $T \in \mathfrak{T}_h$

$$\int_e j_h^3 \cdot n_e q = \int_e g_e q, \quad \forall q \in \mathbb{P}_1(e), \quad \int_T j_h^3 \nabla w = \int_T a \nabla u_h \nabla w, \quad \forall w \in \mathbb{P}_1(T).$$

The global error estimator η_h^i is now given in terms of its elementwise contributions, i.e., $(\eta_h^i)^2 = \sum_{T \in \mathfrak{T}_h} (\eta_h^i(T))^2$, where $\eta_h^i(T)$ is given by means of j_h^i:

$$\eta_h^i(T) = \|a^{-1/2}(a \nabla u_h - j_h^i)\|_T. \tag{3.3}$$

To get suitable bounds, we have to consider additionally the oscillation term given by

$$(\mathrm{osc}_h^i)^2 = \sum_{T \in \mathfrak{T}_h} \mathrm{osc}_h^i(T)^2, \quad \mathrm{osc}_h^i(T) = \alpha_T \|(I - \Pi_h^i)(f - u_h)\|_T,$$

where $\alpha_T = \min\{1, h_T a_T^{-1/2}\}$. We note that if h_T tends to zero, the minimum will be given by $h_T a_T^{-1/2}$.

Remark 3.1. If f is smooth and if $\min_j a_j$ does not tend to zero, osc_h^i is asymptotically a higher order term and thus can be neglected asymptotically. Indeed a standard scaling argument yields $\|(I-\Pi_h^i)(f-u_h)\|_T \lesssim h_T\|\nabla(f-u_h)\|_T$, and therefore

$$\sum_{T\in\mathcal{T}_h}\alpha_T^2\|(I-\Pi_h^i)(f-u_h)\|_T^2 \lesssim \sum_{T\in\mathcal{T}_h} h_T^2 a_T^{-1}\|(I-\Pi_h^i)(f-u_h)\|_T^2 \lesssim \sum_{T\in\mathcal{T}_h} h_T^4 a_T^{-1}\|\nabla(f-u_h)\|_T^2.$$

This shows that

$$\sum_{T\in\mathcal{T}_h}\alpha_T^2\|(I-\Pi_h^i)(f-u_h)\|_T^2 \lesssim \sum_{T\in\mathcal{T}_h} h_T^4 a_T^{-1}\|\nabla f\|_T^2 + \sum_{T\in\mathcal{T}_h} h_T^4 a_T^{-1}\|\nabla u_h\|_T^2. \tag{3.4}$$

But from the discrete variational formulation (2.3) we have

$$\int_\Omega (a|\nabla u_h|^2 + |u_h|^2) = \int_\Omega f u_h.$$

By Cauchy — Schwarz's inequality, we get

$$\int_\Omega (a|\nabla u_h|^2 + |u_h|^2) \leqslant \|f\|_\Omega \|u_h\|_\Omega.$$

This first yields $\|u_h\|_\Omega \leqslant \|f\|_\Omega$, and then $\int_\Omega a|\nabla u_h|^2 \leqslant \|f\|_\Omega^2$. This last estimate implies that

$$(\min_j a_j)\int_\Omega |\nabla u_h|^2 \leqslant \|f\|_\Omega^2,$$

and inserting this estimate into (3.4), we conclude that

$$\mathrm{osc}_h^i \lesssim h^2\{(\min_j a_j)^{-1/2}\|\nabla f\|_\Omega + (\min_j a_j)^{-1}\|f\|_\Omega\}. \tag{3.5}$$

We note that for $\min_j a_j \ll 1$ and coarse meshes the case $i=3$ might be more attractive than the cases $i=1,2$ since the second term of this right-hand side is not present for $i=3$.

3.1. Upper bound for the discretization error. The proof of the upper bound is basically based on the observation that all our fluxes j_h^i are $H(\mathrm{div})$-conforming elements and on the following projection lemma.

Lemma 3.1. $\mathrm{div} j_h^i - \Pi_h^i u_h = -\Pi_h^i f$.

Proof. We start with the observation that $\mathrm{div} V_h^i = W_h^i$. Using the definition (2.4) of g_e and of j_h^i, we find for $w \in W_h^i$

$$\int_\Omega (\mathrm{div} j_h^i - \Pi_h^i u_h)w = \sum_{T\in\mathcal{T}_h}\left(\int_{\partial T} j_h\cdot n_T w - \int_T j_h^i\nabla w - \int_T u_h w\right) =$$

$$\sum_{T\in\mathcal{T}_h}\left(\int_{\partial T} g_T w - \int_T a\nabla u_h\nabla w - \int_T u_h w\right) = -(f,w).$$

□

Theorem 3.1. *The energy norm of the discretization error is bounded by the estimator η_h^i, $i=1,2,3$, and the data oscillation, namely*

$$|||u-u_h||| \leqslant \eta_h^i + \mathrm{osc}_h^i. \tag{3.6}$$

Proof. Using the definition of the energy norm, inserting the $H(\mathrm{div})$-conforming flux, applying Green's formula and Lemma 3.1, we find

$$|||u-u_h|||^2 = \int_\Omega a\nabla(u-u_h)\nabla(u-u_h) + \int_\Omega (u-u_h)(u-u_h) =$$

$$\int_\Omega (j_h^i - a\nabla u_h)\nabla(u-u_h) + \int_\Omega [(I-\Pi_h^i)(f-u_h)](u-u_h).$$

Cauchy — Schwarz's inequality yields

$$\int_\Omega (j_h^i - a\nabla u_h)\nabla(u-u_h) \leqslant \sum_{T\in\mathcal{T}_h} \|a^{-1/2}(j_h^i - a\nabla u_h)\|_T |||u-u_h|||_T = \sum_{T\in\mathcal{T}_h} \eta_{T,1}^i |||u-u_h|||_T,$$

where $|||\cdot|||_T$ stands for the contribution of the energy norm restricted to the element T. We note that $\|w-\Pi_h^i w\|_T \leqslant \|w-\Pi_h^1 w\|_T \leqslant h_T\|\nabla w\|_T$, $w\in H^1(T)$ (see, e.g., Lemma 3.5 of [20]). Then it is easy to see that the second term can be bounded by

$$\int_\Omega [(I-\Pi_h^i)(f-u_h)](u-u_h) \leqslant \sum_{T\in\mathcal{T}_h} \alpha_T \|(I-\Pi_h^i)(f-u_h)\|_T |||u-u_h|||_T \leqslant \mathrm{osc}_h^i |||u-u_h|||.$$

Taking into account the definition of η_h^i, we find

$$|||u-u_h|||^2 \leqslant \sum_{T\in\mathcal{T}_h} \eta_h^i(T)|||u-u_h|||_T + \mathrm{osc}_h^i |||u-u_h||| \leqslant (\eta_h^i + \mathrm{osc}_h^i)|||u-u_h|||.$$

□

Remark 3.2. Note that our upper bound is independent of the shape regularity of the mesh. More precisely it also holds for so-called anisotropic meshes, i.e., meshes for which σ tends to zero as the mesh size h goes to zero.

3.2. Local upper bound for the discretization error. To show that the error estimator is locally bounded by the discretization error and higher order terms, we apply a suitable norm equivalence for mixed finite elements. Define for each element $T\in\mathcal{T}_h$ the quantities $m_{\partial T}(\cdot)$ and $m_T(\cdot)$ by

$$m_{\partial T}(v) = \|v\cdot n_T\|_{\partial T}, \quad m_T(v) = \|\int_T v\|_2, \tag{3.7}$$

where $\|\cdot\|_2$ denotes the Euclidean norm for vectors or matrices. We note that the two quantities are well defined if, e.g., the components of v are polynomials.

Lemma 3.1. *Let $v_h\in V^i(T)$, $T\in\mathcal{T}_h$, then*

$$\|v_h\|_T \sim \left(h_T^{1/2} m_{\partial T}(v_h) + \frac{\beta_i}{h_T} m_T(v_h)\right), \tag{3.8}$$

where $\beta_1=\beta_2=0$ and $\beta_3=1$.

Proof. For convenience of the reader, we sketch the basic steps of the proof. Using the reference element $\widehat{T}$ with vertices $(0,0)$, $(1,0)$ and $(0,1)$, we find for $\hat{v}_h \in V^i(\widehat{T})$ that

$$\|\hat{v}_h\|_{\widehat{T}} \sim (m_{\partial\widehat{T}}(\hat{v}_h) + \beta_i m_{\widehat{T}}(\hat{v}_h)).$$

This simply follows from the fact that all norms on finite dimensional spaces are equivalent. Now we can use the Piola transformation to define for $v_h \in V^i(T)$ the corresponding $\hat{v}_h \in V^i(\widehat{T})$ by

$$\hat{v}_h(\widehat{\boldsymbol{x}}) = \det B_T B_T^{-1} v_h(\boldsymbol{x}),$$

where $\widehat{T}$ is mapped onto T by the affine mapping $\boldsymbol{x} = B_T\widehat{\boldsymbol{x}} + b_T$ and $B_T \in \mathbb{R}^{2\times 2}$ and $b_T \in \mathbb{R}^2$. We recall that $\|B_T\|_2 \sim |\det B_T|\ \|B_T^{-1}\|_2 \sim h_T$ and $|\det B_T| \sim h_T^2$. Then it is easy to see that $\|v_h\|_T \sim \|\hat{v}_h\|_{\widehat{T}}$. Using the relation $\|B_T^{-\top} n_{\widehat{T}}\|_2 n_T = B_T^{-\top} n_{\widehat{T}}$, we find $\det B_T \|B_T^{-\top} n_{\widehat{T}}\|_2 v_h \cdot n_T = \hat{v}_h \cdot n_{\widehat{T}}$ and thus $\|v_h \cdot n_T\|_{\partial T}^2 \sim h_T^{-1} \|\hat{v}_h \cdot n_{\widehat{T}}\|_{\partial\widehat{T}}^2$. For the volume integral we find $\int_T v_h = B_T \int_{\widehat{T}} \hat{v}_h$ and thus $\| \int_T v_h\|_2 \sim h_T \| \int_{\widehat{T}} \hat{v}_h\|_2$. □

With this lemma, we are able to provide an upper bound for $\eta_h^i(T)$.

Lemma 3.2. *For each element $T \in \mathcal{T}_h$ and $i = 1, 2, 3$ we have*

$$\eta_h^i(T) \leqslant \frac{\sqrt{h_T}}{\sqrt{a_T}} \|a_T \nabla u_h \cdot n_T - g_T\|_{\partial T}. \tag{3.9}$$

Proof. The proof is based on the discrete norm equivalence given in Lemma 3.1 and the observation that $a_T \nabla u_h \in V^i(T)$ for $i = 1, 2, 3$. Using the definition of the flux j_h^i and of β_i, we find $\beta_i m_T(j_h^i - a_T \nabla u_h) = 0$. Then, the norm equivalence (3.8) yields

$$\eta_h^i(T) \leqslant \frac{\sqrt{h_T}}{\sqrt{a_T}} m_{\partial T}(a\nabla u_h - j_h^i) = \frac{\sqrt{h_T}}{\sqrt{a_T}} \|a_T \nabla u_h \cdot n_T - j_h^i \cdot n_T\|_{\partial T}.$$

Next, we observe that $(a_T \nabla u_h - j_h^i) \cdot n_e \in S^i(e)$, where $S^1(e) = \mathbb{P}_0(e)$ and $S^2(e) = S^3(e) = \mathbb{P}_1(e)$. Let $\Pi_{\partial T}^i$ be the L^2-projection onto $S^i(\partial T) := \prod_{e\subset\partial T} S^i(e)$, then $\Pi_{\partial T}^i(a_T \nabla u_h \cdot n_T) = a_T \nabla u_h \cdot n_T$ and $j_h^i \cdot n_T = \Pi_{\partial T}^i(j_h^i \cdot n_T) = \Pi_{\partial T}^i g_T$. Here we have used the definition of j_h^i and the fact that $j_h^i \cdot n_T \in S^i(\partial T)$. These preliminary considerations give now the upper bound

$$\eta_h^i(T) \leqslant \frac{\sqrt{h_T}}{\sqrt{a_T}} \|\Pi_{\partial T}^i (a_T \nabla u_h \cdot n_T - g_T)\|_{\partial T} \leqslant \frac{\sqrt{h_T}}{\sqrt{a_T}} \|a_T \nabla u_h \cdot n_T - g_T\|_{\partial T}.$$

□

Theorem 3.2. *For each element $T \in \mathcal{T}_h$ the estimate*

$$\eta_h^i(T) \leqslant \left(\max_{T'\subset\omega_T} \left\{ \frac{\sqrt{a_{T'}}}{\sqrt{a_T}} \right\} \right) \left(\max_{T'\subset\omega_T} \max\{1, h_{T'} a_{T'}^{-1/2}\} \right) \left(|||u - u_h|||_{\omega_T} + \sum_{T'\subset\omega_T} \operatorname{osc}_h^1(T) \right), \tag{3.10}$$

holds, where ω_T denotes the patch consisting of all the triangles of $\mathcal{T}_h$ sharing a vertex with T.

Proof. The right-hand side of (3.9) is bounded by the edge contributions $\sqrt{h_e}/\sqrt{a_T}\|a_T \nabla u_h \cdot n_e - g_e\|_e^2$ which is a part of the equilibrated error estimator that can be bounded in terms of the discretization error. Theorem 6.2 of [1] yields

$$\sum_{e\subset\partial T} h_e \|a_T \nabla u_h \cdot n_e - g_e\|_e^2 \leqslant \sum_{T'\subset\omega_T} h_{T'}^2 \|R_{T'}\|_{T'}^2 + \sum_{e\subset\omega_T} h_e \|J_{e,n}\|_e^2,$$

where $R_T = f + \operatorname{div}(a\nabla u_h) - u_h$ is the exact residual on the element T and $J_{e,n}$ stands for the jump of the flux over edges :

$$J_{e,n} = \begin{cases} \left[\!\left[a\nabla u_h \cdot n_e\right]\!\right]_e, & \text{for interior edges,} \\ 0, & \text{for Dirichlet boundary edges,} \\ \nabla u_h \cdot n_e, & \text{for Neumann boundary edges.} \end{cases}$$

Introducing, for an edge e, $a_e = \max\{a_{T_1}, a_{T_2}\}$, $e = \partial T_1 \cap \partial T_2$ we get

$$\eta_h^i(T)^2 \leqslant a_T^{-1} \max_{T'\subset\omega_T}\{a_{T'}\}\left(\sum_{T'\subset\omega_T} a_{T'}^{-1}h_{T'}^2\|R_{T'}\|_{T'}^2 + \sum_{e\subset\omega_T} a_e^{-1}h_e\|J_{e,n}\|_e^2\right). \tag{3.11}$$

The residual and the jump are terms appearing in the residual-based error estimator. It is well known (see, e.g., [23]), that these terms can be locally bounded by the error. Introducing element and edge bubble functions, we can bound, by inverse inequalities, those terms by local contributions of the discretization error. □

Remark 3.1. Note that in estimate (3.10) we give the exact dependence of the constant with respect to the coefficients a_j. Hence, if $\min_j a_j$ goes to zero or if $\max_{j,j'}(a_j/a_{j'})$ goes to infinity, the constant

$$C(a) := \left(\max_T \max_{T'\subset\omega_T}\left\{\frac{\sqrt{a_{T'}}}{\sqrt{a_T}}\right\}\right)\left(\max_{T'\subset\omega_T} \max\{1, a_{T'}^{-1/2}\}\right) = \left(\max_{j,j'}\frac{\sqrt{a_j}}{\sqrt{a_{j'}}}\right)\max\{1, \max_j a_j^{-1/2}\}$$

will blow up.

4. Convergence of the adaptive algorithm

In this section, we show that a bulk-type marking strategy (see, e.g., [9,13,16,18]), based here on the refinement procedure REFINE of Morin, Nochetto and Siebert [13, 16, 17], leads to the convergence of the corresponding adaptive algorithm. Note that this procedure requires the interior node property. In the very recent results from [6], this property was suppressed, but, unfortunately, we are not able to adapt their proof to our setting.

Here, in order to obtain oscillation and error reductions, we take

$$(\operatorname{osc}_h)^2 = \sum_{T\in\mathcal{T}_h} \operatorname{osc}_h(T)^2, \quad \operatorname{osc}_h(T) = h_T a_T^{-1/2}\|(I - \Pi_h^1)(f - u_h)\|_T.$$

Let us notice that all the results of the previous section are valid for this choice.

Now we recall the marking strategy of the bulk type.

Definition 4.1 (Marking strategy). Let $i \in \{1, 2, 3\}$ be fixed. Given two parameters $0 < \theta_1, \theta_2 < 1$, the new family $\mathcal{T}_h$ is designed with the help of a subset of marked elements $\hat{T}_H$ of $\mathcal{T}_H$ constructed so that

$$\sum_{T\in\hat{T}_H} \eta_H^i(T)^2 \geqslant \theta_1^2(\eta_H^i)^2, \tag{4.1}$$

$$\sum_{T\in\hat{T}_H} \operatorname{osc}_H(T)^2 \geqslant \theta_2^2\operatorname{osc}_H^2. \tag{4.2}$$

Note that these two conditions yield

$$\sum_{T\in\hat{T}_H} (\eta_H^i(T)^2 + \mathrm{osc}_H(T)^2) \geqslant \theta^2((\eta_H^i)^2 + \mathrm{osc}_H^2), \tag{4.3}$$

with $\theta = \min\{\theta_1, \theta_2\}$.

Now we can prove the convergence result.

Theorem 4.1. *Assume that the successive meshes are constructed via the procedure REFINE of Morin, Nochetto and Siebert* [13, 16, 17] *and that the marking strategy is the one from Definition* 4.1 *by using the estimator* η_H^i *and the oscillating term* osc_H *defined in this section for a fixed* $i = 1, 2$ *or* 3. *Then there exist two constants* $\kappa > 0$ *and* $0 < \mu < 1$ *such that*

$$|||u - u_h|||^2 + \kappa \mathrm{osc}_h^2 \leqslant \mu(|||u - u_H|||^2 + \kappa \mathrm{osc}_H^2), \tag{4.4}$$

where $h < H$ *are two consecutive mesh parameters. The constant* μ *tends to* 1 *as* $C(a)$ *tends to infinity.*

Proof. The proof is similar to that for the proof of Theorem 1.1 of [13]. Since we further want to trace the dependence of the constant μ with respect to the parameters a_j, we give the details.

First, we clearly have the orthogonality relation

$$B(u - u_h, u - u_h) = B(u - u_H, u - u_H) - B(u_h - u_H, u_h - u_H), \tag{4.5}$$

since the bilinear form B is symmetric and the Galerkin orthogonality relation

$$B(u - u_h, v_h) = 0 \quad \forall v_h \in X_h,$$

holds (as $X_h \subset H_D^1(\Omega)$). The upper bound was proved in Theorem 3.1. The oscillation reduction estimate follows from Lemma 3.2 of [13], namely it was proved that, under the marking strategy (4.2), there exist two constants $0 < \rho_1 < 1$ and $\rho_2 > 0$ independent of h such that

$$\mathrm{osc}_h^2 \leqslant \rho_1 \mathrm{osc}_H^2 + \rho_2 |||u_h - u_H|||^2. \tag{4.6}$$

It then remains to show the error reduction estimate:

$$\sum_{T\in\hat{T}_H} \eta_H(T)^2 \leqslant C_1(|||u_h - u_H|||^2 + \mathrm{osc}_H^2). \tag{4.7}$$

But we notice that for any marked element $T \in \hat{T}_H$ using element and edge bubble functions in X_h associated with an interior node of $\mathcal{T}$ in T or in one of its edges, we can show, as in the proof of Theorem 3.2, that

$$\eta_H(T)^2 \leqslant C(a)(|||u_h - u_H|||_{\omega_T}^2 + \mathrm{osc}_H(T)^2),$$

and by superposition we conclude that (4.7) holds with $C_1 \sim C(a)$.

Using the error reduction estimate (4.7), we obtain

$$\sum_{T\in\hat{T}_H} \eta_H(T)^2 \leqslant C_1(|||u_h - u_H|||^2 + \mathrm{osc}_H^2). \tag{4.8}$$

Applying the upper bound (3.6) to the rough mesh parameter H, and secondly using the marking procedures (4.1) and (4.2), we have

$$\theta^2 |||u - u_H|||^2 \leqslant \theta^2 \Big(\sum_{T \in \mathcal{T}_H} \eta_T(u_H)^2 + \mathrm{osc}_H^2 \Big) \leqslant \sum_{T \in \hat{T}_H} \eta_T(u_H)^2 + \sum_{T \in \hat{T}_H} \mathrm{osc}_H(T)^2.$$

Using now estimate (4.8), we arrive at

$$\theta^2 |||u - u_H|||^2 \leqslant C_1 |||u_h - u_H|||^2 + (1 + C_1)\mathrm{osc}_H^2,$$

or equivalently

$$|||u_h - u_H|||^2 \geqslant \frac{\theta^2}{C_1} |||u - u_H|||^2 - C_2 \mathrm{osc}_H^2, \tag{4.9}$$

with $C_2 = 1 + C_1^{-1}$.

Now, using the orthogonality relation (4.5) and the property $B(u,u) = |||u|||^2$ and introducing a parameter $\beta \in (0,1)$ fixed sufficiently small later on, we obtain

$$|||u - u_h|||^2 = |||u - u_H|||^2 + (\beta - 1) |||u_h - u_H|||^2 - \beta |||u_h - u_H|||^2.$$

The last term of this right-hand side is estimated by invoking (4.9), and therefore

$$|||u - u_h|||^2 \leqslant |||u - u_H|||^2 + (\beta - 1) |||u_h - u_H|||^2 - \frac{\theta^2 \beta}{C_1} |||u - u_H|||^2 + \beta C_2 \mathrm{osc}_H^2,$$

or equivalently

$$|||u - u_h|||^2 \leqslant \left(1 - \frac{\theta^2 \beta}{C_1}\right) |||u - u_H|||^2 + (\beta - 1) |||u_h - u_H|||^2 + \beta C_2 \mathrm{osc}_H^2. \tag{4.10}$$

To take into account the oscillating terms, we multiply (4.6) by $\kappa := (1 - \beta)/\rho_2$ and find

$$\kappa \mathrm{osc}_h^2 \leqslant \kappa \rho_1 \mathrm{osc}_H^2 + (1 - \beta) |||u_h - u_H|||^2. \tag{4.11}$$

The sum of the estimates (4.10) and (4.11) yields

$$|||u - u_h|||^2 + \kappa \mathrm{osc}_h^2 \leqslant \left(1 - \frac{\theta^2 \beta}{C_1}\right) |||u - u_H|||^2 + (\kappa \rho_1 + \beta C_2)\, \mathrm{osc}_H^2.$$

This estimate leads to the conclusion if we can choose β small enough so that there exists $0 < \mu < 1$ such that

$$1 - \frac{\theta^2 \beta}{C_1} \leqslant \mu, \quad \kappa \rho_1 + \beta C_2 \leqslant \mu \kappa.$$

It is always possible to find $\mu \in (0,1)$ such that the first estimate holds. On the other hand the second estimate is equivalent to (using the definition of κ)

$$\rho_1 + \frac{C_2 \beta \rho_2}{1 - \beta} \leqslant \mu. \tag{4.12}$$

To guarantee estimate (4.12), we simply choose β small enough such that

$$\rho_1 + \frac{C_2 \beta \rho_2}{1 - \beta} < 1,$$

which is equivalent to

$$\frac{\beta}{1-\beta} < \frac{1-\rho_1}{C_2\rho_2},$$

which is always possible since the left-hand side of this estimate tends to zero as β goes to zero.

Hence with such a choice of β, estimate (4.12) holds with $1 > \mu \geqslant \rho_1 + C_2\beta\rho_2/(1-\beta)$.

We conclude by the choice $\mu = \max\{\rho_1 + C_2\beta\rho_2/(1-\beta);\ 1-\theta^2\beta/C_1\}$. With this choice, we directly see that if $C(a)$ tends to infinity, then $1-\theta^2\beta/C_1$ tends to 1, which implies the convergence of μ to 1. □

5. Numerical results

Our first example consists in solving Eq. (2.1) on the unit square $\Omega = (0,1)^2$ with $\Gamma_N = \Gamma$. The coefficient a is fixed to be constant and equal to 1. We take isotropic meshes composed of triangles, and we compute j_h^i, $i = 1,2,3$. The test is performed with different types of solutions. In the first case, we consider the exact solution

$$u(x,y) = \frac{1}{2}\cos(\pi x)\cos(\pi y). \tag{5.1}$$

To begin, we check that the numerical solution u_h converges toward the exact solution. To this end, we plot the curve $|||u-u_h|||$ (and the estimators) as a function of DoF (see Fig. 5.1). We see that the approximate solution converges toward the exact one with an experimental convergence rate of one (for its exact definition see below) and that the estimators are very close to the error (see Figs. 5.1 and 5.2). In all our test settings, we find that the inverse of the effectivity indices, i.e., the ratios $|||u-u_h|||/\eta_h^i$, are smaller than one. Indeed, we remark in Fig. 5.2 that they vary between 0.67 and 0.87, in other words, they remain smaller than one.

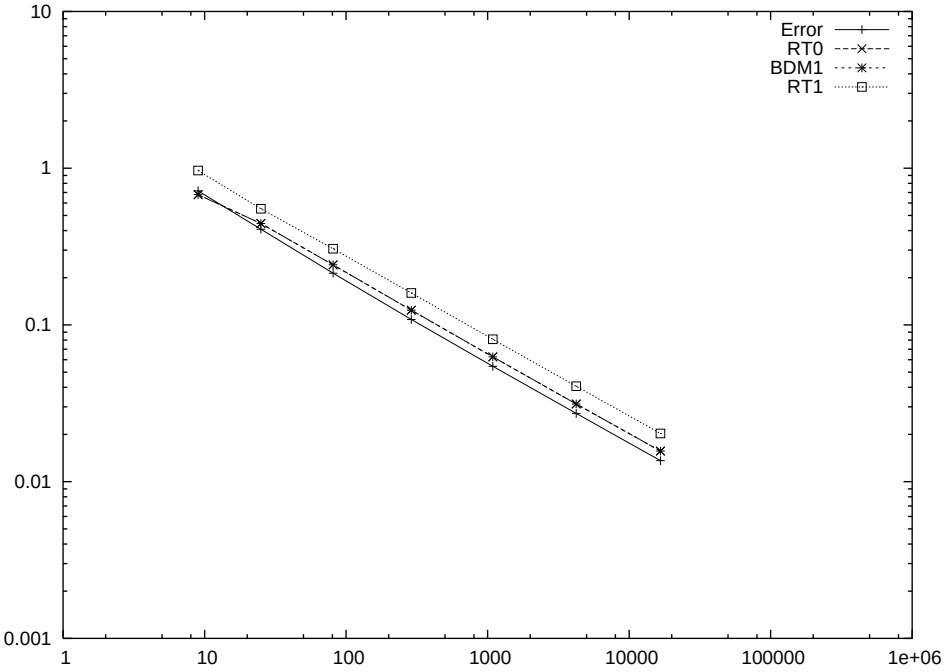

Fig. 5.1. $|||u-u_h|||$ and η_h^i, $i = 1,2,3$ wrt DoF for the first solution

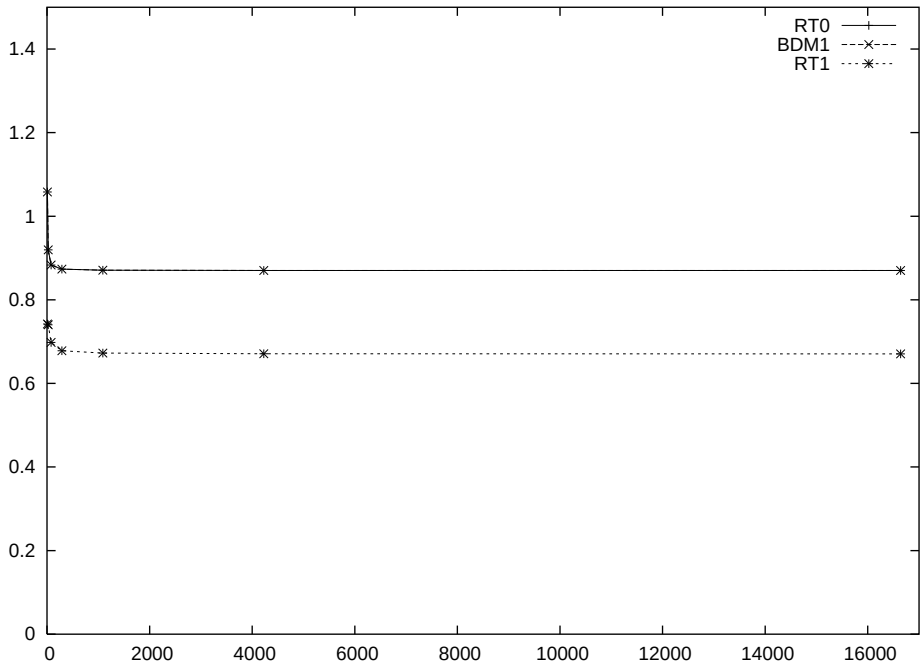

Fig. 5.2. Ratios $|||u - u_h|||/\eta_h^i$, $i = 1, 2, 3$ wrt DoF for the first solution

Now we take for the exact solution

$$u(x, y) = e^{(3x^2-2x^3+3y^2-2y^3)}. \tag{5.2}$$

As before, Fig. 5.3 shows the error and the estimators wrt the DoF and Fig. 5.4 gives the inverse of the effectivity indices. Here we can draw the same conclusion as before, except that the effectivity indices are even larger.

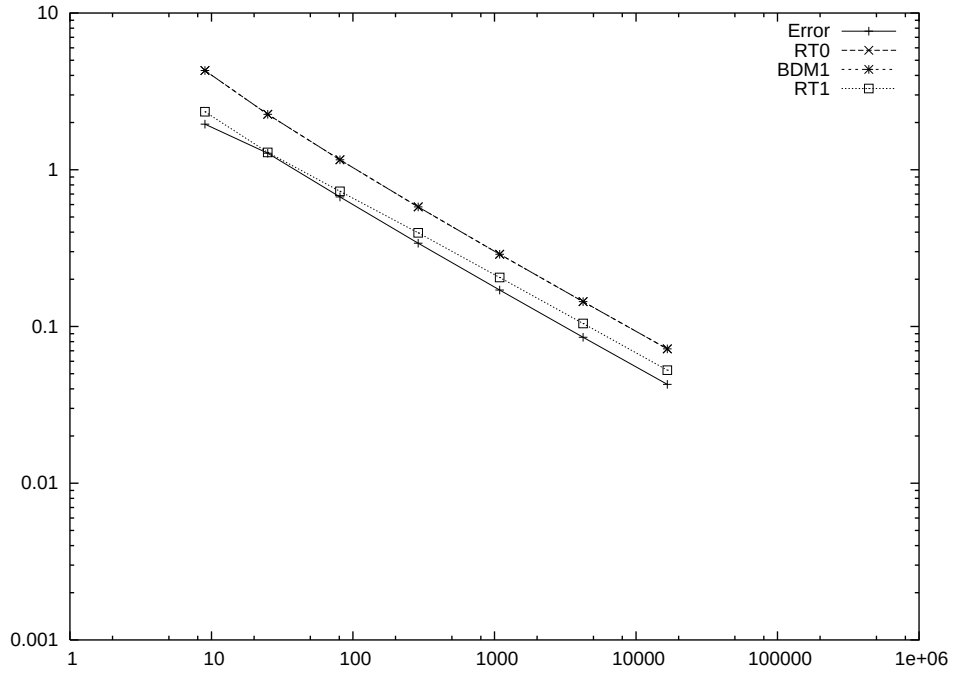

Fig. 5.3. $|||u - u_h|||$ and η_h^i, $i = 1, 2, 3$ wrt DoF for the second solution

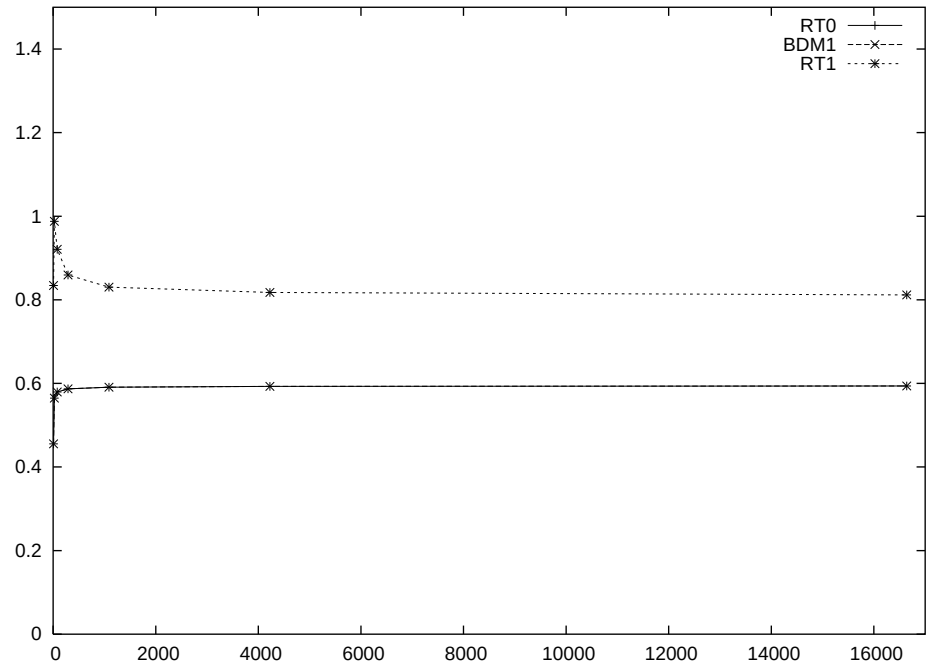

Fig. 5.4. Ratios $|||u - u_h|||/\eta_h^i$, $i = 1, 2, 3$ wrt DoF for the second solution

Now, we consider a solution of problem (2.1) on the unit square $\Omega = (0,1)^2$ with $\Gamma_D = \Gamma$ that exhibits an exponential layer along the y-axis. Namely we take

$$u(x,y) = 4y(1-y)(1 - e^{-\alpha x} - (1 - e^{-\alpha})x) \tag{5.3}$$

with different values of the parameter α, the coefficient in (2.1) being taken as $a = 1/\alpha^2$. Here in order to resolve appropriately the boundary layer of the solution we use anisotropic meshes of the Shishkin type as described in [10, 21] for instance (see Remark 3.2). First, we compute the upper bound $\eta_h^3 + \mathrm{osc}_h^3$ and compare it with the exact error. According to Fig. 5.5, we see a good convergence of the approximate solution to the exact one. Moreover the estimator remains close to the error as far as the mesh size is small enough. This is confirmed by Fig. 5.6 where the ratio $|||u - u_h|||/(\eta_h^3 + \mathrm{osc}_h^3)$ is presented for the four values of α with respect to DoF. Secondly, we have computed the global upper bound $\eta_h^1 + \mathrm{osc}_h^1$ (based on RT_0) and compared it with the exact error and the two contributions η_h^1 and osc_h^1. These comparisons are presented in Figs. 5.7 and 5.8 for $\alpha = 1$ and 10. In Fig. 5.7, we can see that as far as the mesh size is small enough compared to the size of α, the term osc_h^1 is much smaller than η_h^1, as expected theoretically (see Remark 3.1). Vice versaa if the mesh size is relatively rough compared to the size of α, the term osc_h^1 is comparable with η_h^1 (see Fig. 5.7, right). Note further that the use of η_h^1 is more time consuming than η_h^3 since we were unable to achieve the value of $h = 1/128$ for $\alpha = 100$ and 1000 in a reasonable time.

Now, in order to illustrate the performance of our estimator η_h^3, for three examples taken from [12] we show the meshes obtained after some iterations, as well as some quantities of main interest during different iterations. We use the bulk-type iteration algorithm described in Definition 4.1 with $\theta_1 = \theta_2 = \theta = 0.75, 0.8$ or 0.9 and refine the triangles of $\hat{T}_H$ by the standard refinement procedure with a limitation on the minimal angle.

For all the examples we show the meshes obtained after some iterations, as well as the experimental convergence orders of the error

$$EOC_e = 2\frac{\lg(|||u - u_H|||/|||u - u_h|||)}{\lg(DOF_h/DOF_H)},$$

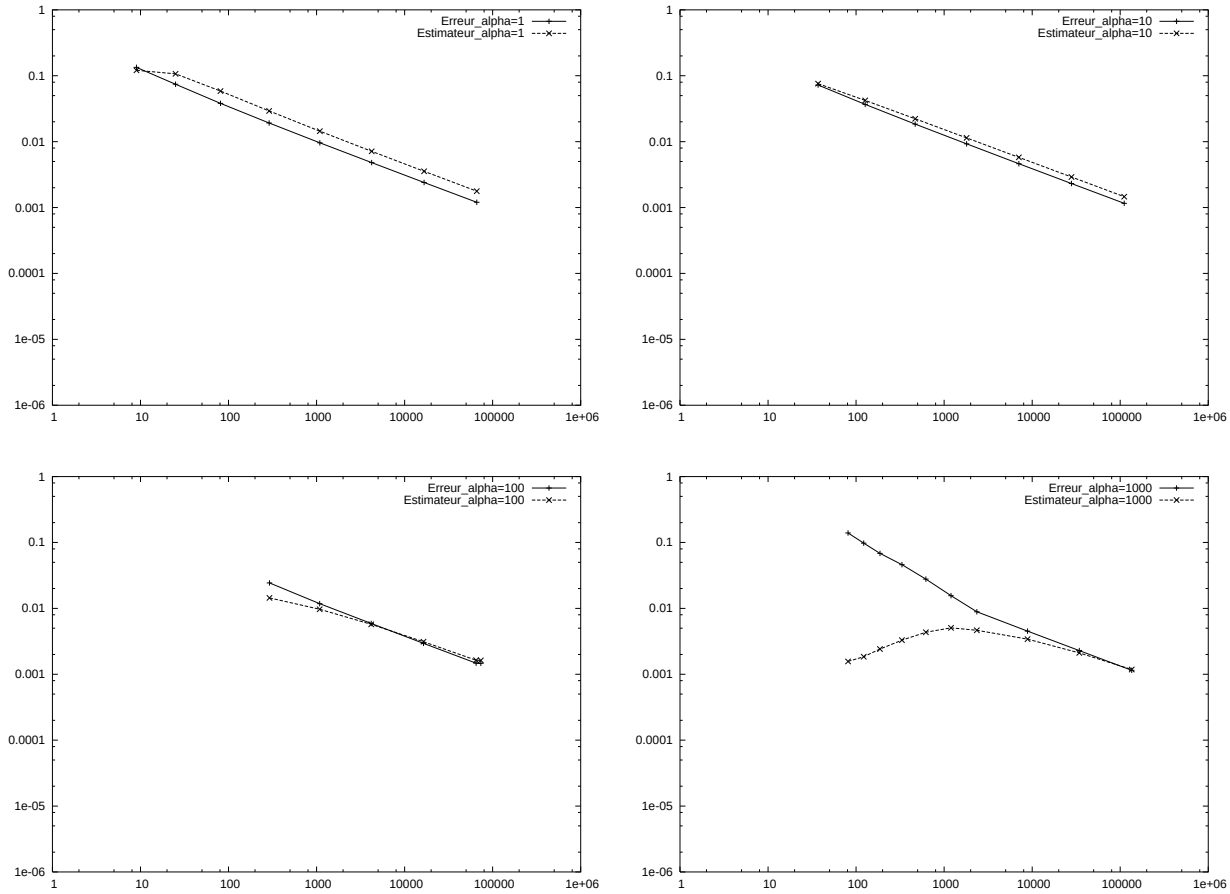

Fig. 5.5. $|||u-u_h|||$ and $\eta_h^3+\mathrm{osc}_h^3$ wrt DoF for different values of α: top-left: $\alpha=1$, top-right $\alpha=10$; bottom-left $\alpha=100$, bottom-right $\alpha=1000$

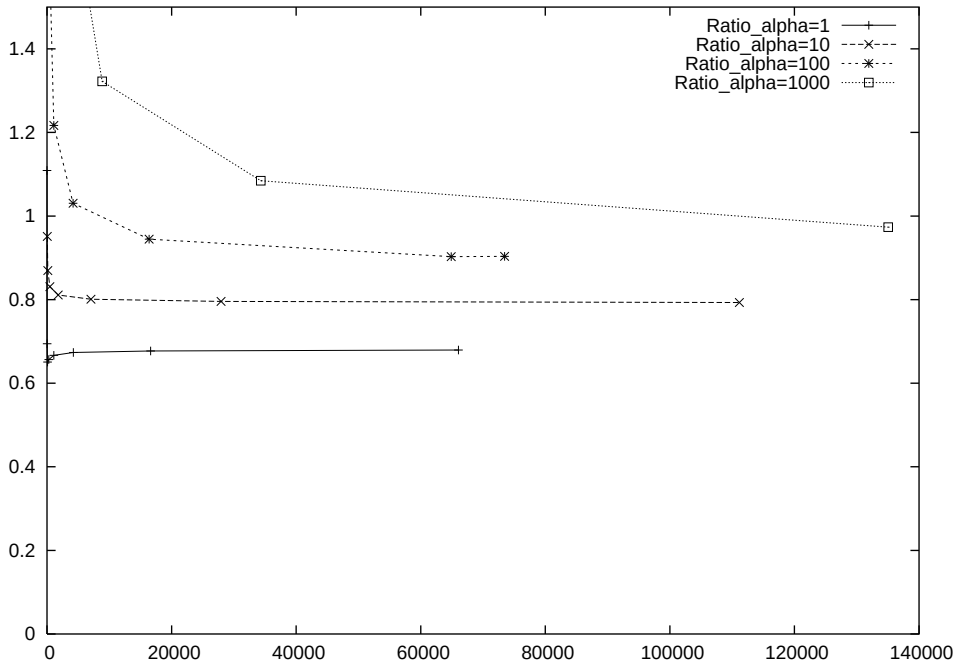

Fig. 5.6. Ratio $|||u-u_h|||/(\eta_h^3+\mathrm{osc}_h^3)$ wrt DoF for different values of α

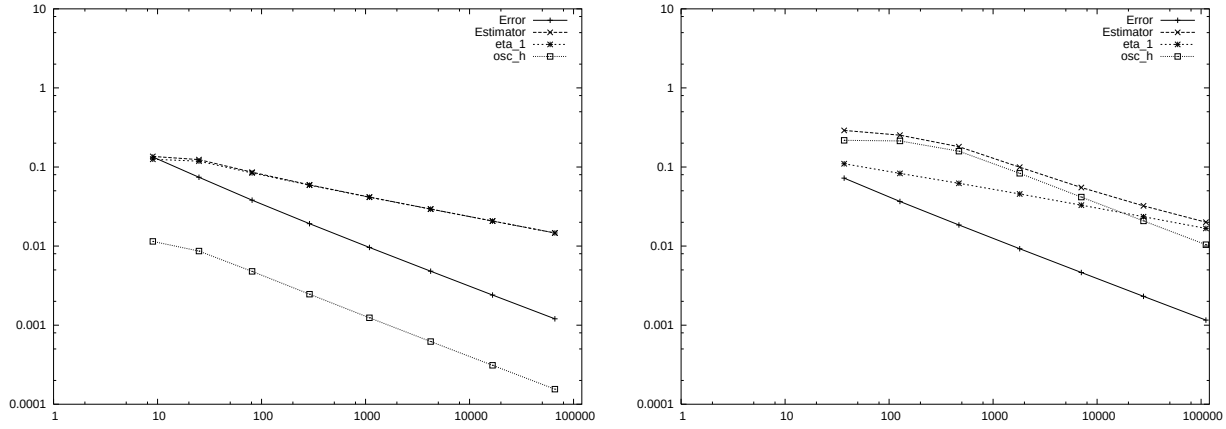

F i g. 5.7. $|||u-u_h|||$, $\eta_h^1+\mathrm{osc}_h^1$, η_h^1 and osc_h^1 wrt DoF for different values of α: $\alpha=1$ (left) and $\alpha=10$ (right)

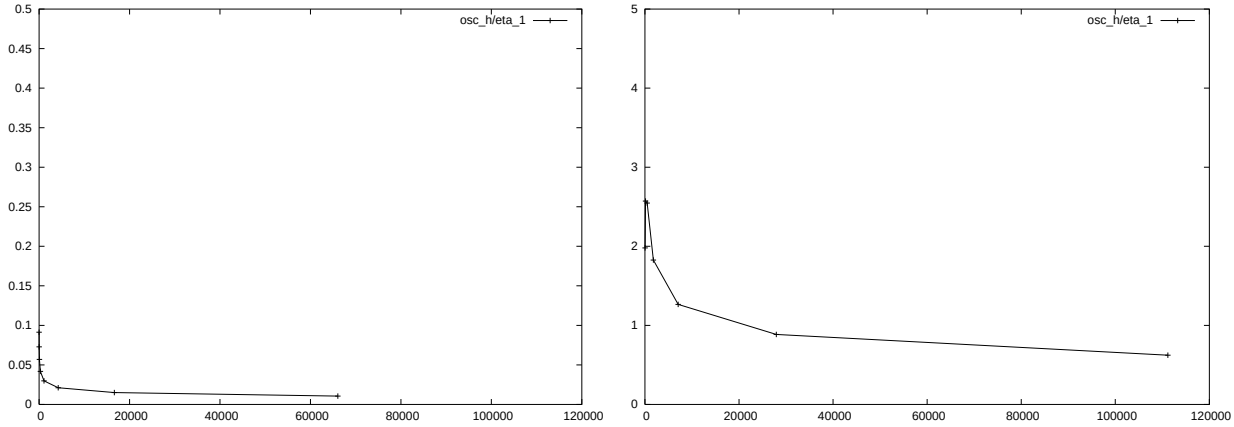

F i g. 5.8. Ratio $\mathrm{osc}_h^1/\eta_h^1$ wrt DoF for different values of α: $\alpha=1$ (left), $\alpha=10$ (right)

the effectivity indices

$$\mathrm{Eff}=\eta_h^3/|||u-u_h|||,$$

and the reduction factors of the error (approximate value of the constant $\sqrt{\mu}$ appearing in Theorem 4.1)

$$\mathrm{RFE}=|||u-u_h|||/|||u-u_H|||,$$

calculated during different iterations.

For the first example we take $\Omega=(0,1)^2$, $a=1$, $\Gamma_D=\Gamma$ and as the exact solution,

$$u(x,y)=x(x-1)y(y-1)e^{(-100(x-1/2)^2-100(y-117/1000)^2)}.$$

This solution has a large gradient around the point $(1/2, 117/1000)$. Therefore a refinement of the mesh near this point can be expected. This is confirmed by Fig. 5.9. Table 5.1 reveals an experimental convergence rate approximately equal to 1. There we can also notice that the effectivity indices vary between 1.03 and 1.26 showing that the oscillating term is already quite small. The reduction factors of the error are around 0.67, which confirms the convergence of the algorithm.

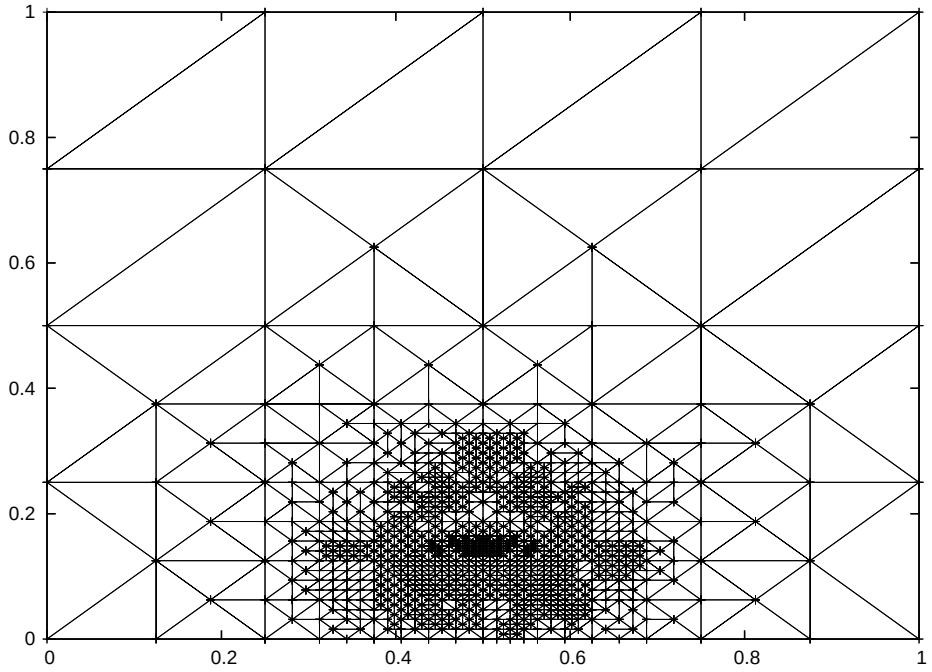

Fig. 5.9. Adaptive mesh after 9 iterations for the first example and the bulk criterion

Table 5.1. **Effectivity indices, reduction factors of the error, and experimental order of convergence of the error for the first example with $\theta = 10.8$**

DOF	Eff	RFE	EOC_e
25	0.237481		
37	1.18759	0.657714	2.13745
49	1.03378	0.810633	1.49475
86	1.03357	0.673846	1.4035
208	1.16428	0.600611	1.15447
435	1.18324	0.625191	1.27323
975	1.16901	0.643145	1.09377
2242	1.18481	0.654676	1.01747
5316	1.22655	0.646628	1.00998
12194	1.23452	0.665001	0.982788
26708	1.24233	0.675700	0.999992
58024	1.26494	0.672237	1.02371

For the second example we consider the checkerboard benchmark. In other words, we take $\Omega = (-1,1)^2$ and $\Gamma_D = \Gamma$ but a discontinuous coefficient a. Namely we decompose Ω into 4 subdomains Ω_i, $i = 1, \ldots, 4$ with

$$\Omega_1 = (0,1) \times (0,1), \quad \Omega_2 = (-1,0) \times (0,1),$$

$$\Omega_3 = (-1,0) \times (-1,0), \quad \Omega_4 = (0,1) \times (-1,0)$$

and take $a = a_i$ on Ω_i, with $a_1 = a_3$ and $a_2 = a_4 = 1$. Using polar coordinates centered at $(0,0)$, we take, as the exact solution,

$$S(x,y) = r^\alpha \phi(\theta), \tag{5.4}$$

where $\alpha \in (0,1)$ and ϕ are chosen such that S is harmonic on each subdomain Ω_i, $i = 1, \ldots, 4$ and satisfies the jump conditions

$$[\![S]\!] = 0 \text{ and } [\![a\nabla S \cdot n]\!] = 0$$

on the interfaces (i.e., the segments $\bar{\Omega}_i \cap \bar{\Omega}_{i+1}$ (mod 4), $i = 1, \ldots, 4$). We fix nonhomogeneous Dirichlet boundary conditions on Γ accordingly.

It is easy to see (see, for instance, [8]) that α is the root of the transcendental equation

$$\tan \frac{\alpha\pi}{4} = \sqrt{a_1}.$$

This solution has a singular behavior around the point $(0,0)$ (because $\alpha < 1$). Therefore a refinement of the mesh near this point can be expected. This can be checked in Figs. 5.10 and 5.11 on the meshes obtained for $a_1 = 5$ and $a_1 = 100$ respectively and for which $\alpha \approx 0.53544094560$ and $\alpha \approx 0.1269020697$. Table 5.2 shows an experimental convergence rate approximatively equal to 0.9 for $a_1 = 5$ and 0.7 for $a_1 = 100$; in this last case the results are less accurate due to the high singular behavior of the solution. There we see that the different effectivity indices are around 1.9 for $a_1 = 5$ and 4 for $a_1 = 100$, which is quite satisfactory. The reduction factors of the error are around 0.75 and 0.9, hence the adaptive algorithms are convergent. We further see that the reduction factors of the error are less good for $a_1 = 100$ than for $a_1 = 5$, which is in accordance with the fact that the constant μ in Theorem 4.1 may deteriorate as $\max_{j,j'} a_j/a_{j'}$ becomes large.

Finally, as the last example, we take the L-shape domain

$$\Omega = (-1,1)^2 \setminus (-1,0) \times (0,1), \quad a = 1, \quad \Gamma_D = \Gamma$$

and as the exact solution

$$S = r^{2/3} \sin(2\theta/3). \tag{5.5}$$

This solution has a singular behavior at $(0,0)$ and the meshes have to be refined near this point. This can be seen in Fig. 5.12. As before, an experimental convergence rate 1 of the error is confirmed by Table 5.3, while effectivity indices of around 2.5 show a good efficiency of the estimator. The reduction factors of the error are around 0.64, which confirms the convergence of the adaptive algorithm.

All these tests confirm the reliability and efficiency of the error estimators proposed by us. Nevertheless for $a \ll 1$ and coarse meshes the estimator η_h^3 based on RT_1 is more attractive and less expensive than the estimators η_h^1 and η_h^2.

Acknowledgement. We are very grateful to E. Creusé (Univ. Lille 1, France) for his help for some numerical tests.

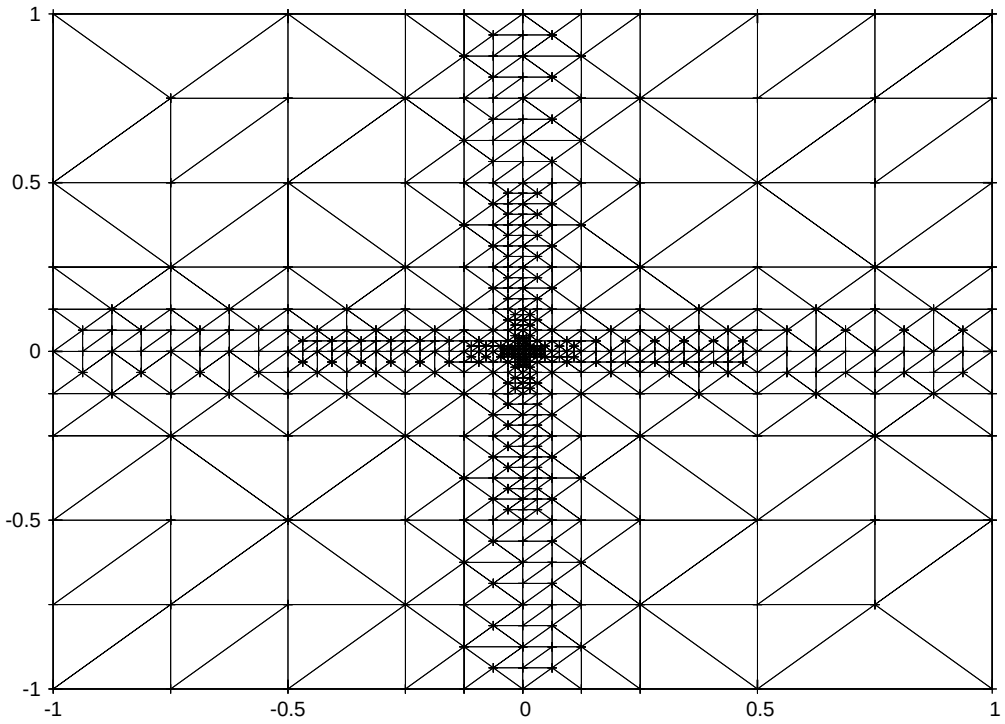

Fig. 5.10. Adaptive mesh after 7 iterations for the second example ($a_1 = 5$ and bulk criterion)

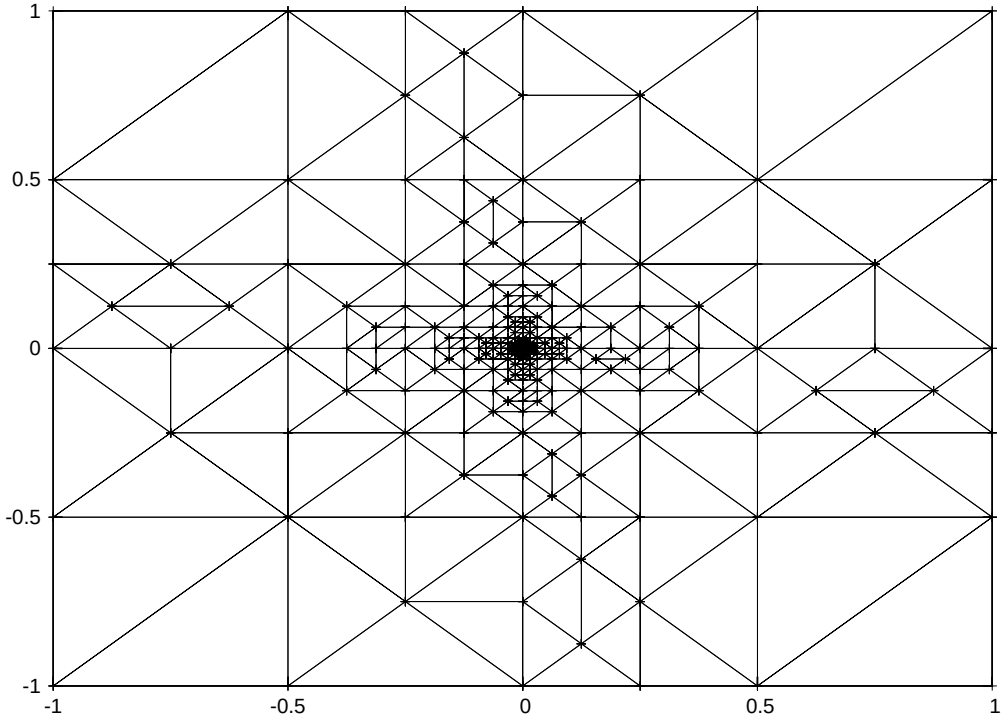

Fig. 5.11. Adaptive mesh after 8 iterations for the second example ($a_1 = 100$ and bulk criterion)

Table 5.2. **Effectivity indices, reduction factors of the error, and experimental convergence rates for the checkerboard with $a_1 = 5, \theta = 0.8$ (left) and $a_1 = 100, \theta = 0.9$ (right)**

DOF	Eff	RFE	EOC_e
25	2.01335		
39	2.14611	0.718651	1.4859
60	2.24146	0.761383	1.26569
95	2.3238	0.75483	1.22412
165	2.2904	0.794549	0.833158
283	2.10819	0.841344	0.640425
521	1.98209	0.812719	0.679563
976	1.86595	0.82385	0.617374
1792	1.87167	0.765401	0.880000
3336	1.9023	0.748037	0.934292
6196	1.89261	0.748703	0.9349

DOF	Eff	RFE	EOC_e
25	4.68157		
30	6.04009	0.869189	1.53789
33	4.71467	0.955182	0.962203
57	4.62601	0.851157	0.589739
94	4.49583	0.859855	0.603671
126	4.46694	0.876004	0.903685
166	4.44417	0.886149	0.876808
217	4.40943	0.892452	0.849407
289	4.3721	0.899012	0.743089
383	4.31752	0.902714	0.726892
507	4.26203	0.905784	0.70562
667	4.21771	0.909483	0.691845
858	4.16205	0.916124	0.695777
1100	4.09904	0.920219	0.669269
1412	4.02756	0.923556	0.636961

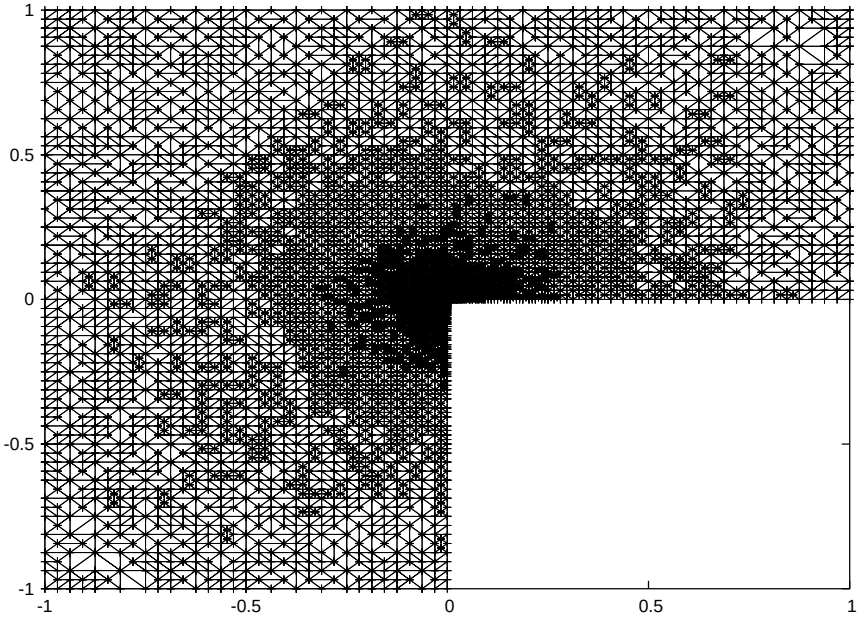

Fig. 5.12. Adaptive mesh after 12 iterations for the third example and the bulk criterion

Table 5.3. **Convergence rates, effectivity indices, and reduction factors of the error for the *L*-shape with $\theta = 0.75$**

DOF	Eff	RFE	EOC_e
21	3.254308		
41	2.893879	0.811498	0.624389
103	2.779986	0.682732	0.828637
275	2.609011	0.66434	0.832878
719	2.576177	0.639566	0.930123
1919	2.518023	0.644163	0.896006
4828	2.510469	0.642127	0.960233
13171	2.476608	0.633977	0.908229
31855	2.467278	0.645789	0.99025
76424	2.507736	0.637029	1.0306

References

1. M. Ainsworth and J. Oden, *A posteriori error estimation in finite element analysis*, John Wiley and Sons, 2000.

2. I. Babuška and T. Strouboulis, *The finite element method and its reliability*, Clarendon Press, Oxford.

3. D. Braess and J. Schöberl, *Equilibrated residual error estimator for edge elements*, Math. Comp., **77** (2008), no. 262, pp. 651–672.

4. S. C. Brenner and L. R. Scott, *The mathematical theory of finite element methods*, Springer, New York, 1994.

5. F. Brezzi and M. Fortin, *Mixed and hybrid finite element methods*, Springer-Verlag, New-York, 1991.

6. M. J. Cascon, C. Kreuzer, R. H. Nochetto, and K. G. Siebert, *Quasi-optimal convergence rate of an adaptive FEM*, SIAM J. Numer. Anal., **46** (2008), no, 5, pp. 2524–2550.

7. P. G. Ciarlet, *The finite element method for elliptic problems*, North-Holland, Amsterdam, 1978.

8. M. Costabel, M. Dauge, and S. Nicaise, *Singularities of Maxwell interface problems*, RAIRO Modél. Math. Anal. Numér., **33** (1999), pp. 627–649.

9. W. Dörfler, *A convergent adaptive algorithm for Poisson's equation*, SIAM J. Numer. Anal., **33** (1996), no. 3, pp. 1106–1124.

10. G. Kunert, *An a posteriori residual error estimator for the finite element method on anisotropic tetrahedral meshes*, Numer. Math., **86** (2000), no. 3, pp. 471–490, DOI 10.1007/s002110000170.

11. P. Ladevèze and D. Leguillon, *Error estimate procedure in the finite element method and applications*, SIAM J. Numer. Anal., **20** (1983), pp. 485–509.

12. R. Luce and B. Wohlmuth, *A local a posteriori error estimator based on equilibrated fluxes*, SIAM J. Numer. Anal., **42** (2004), pp. 1394–1414.

13. K. Mekchay and R. H. Nochetto, *Convergence of adaptive finite element methods for general second order linear elliptic PDEs*, SIAM J. Numer. Anal., **43** (2005), no. 5, pp. 1803–1827.

14. P. Monk, *A posteriori error indicators for Maxwell's equations*, J. Comput. Appl. Math., **100** (1998), pp. 73–190.

15. P. Monk, *Finite element methods for Maxwell's equations*, Numerical Mathematics and Scientific Computation. Oxford University Press, 2003.

16. P. Morin, R. H. Nochetto, and K. G. Siebert, *Data oscillation and convergence of adaptive FEM*, SIAM J. Numer. Anal., **38** (2000), no. 2, pp. 466–488.

17. P. Morin, R. H. Nochetto, and K. G. Siebert, *Convergence of adaptive finite element methods*, SIAM Rev., **44** (2003), no. 4, pp. 631–658, 2002. Revised reprint of "Data oscillation and convergence of adaptive FEM", SIAM J. Numer. Anal. **38** (2000), no. 2, pp. 466–488, MR1770058 (2001g:65157).

18. P. Morin, R. H. Nochetto, and K. G. Siebert, *Local problems on stars: a posteriori error estimators, convergence, and performance*, Math. Comp., **72** (2003), no. 243, pp. 1067–1097.

19. P. Neittaanmaäki and S. Repin, *Reliable methods for computer simulation: error control and a posteriori error estimates*, vol. 33 of *Studies in Mathematics and its applications*, Elsevier, Amsterdam, 2004.

20. S. Nicaise, *A posteriori error estimations of some cell centered finite volume methods*, SIAM J. Numer. Anal., **43** (2005), pp. 1481–1503.

21. S. Nicaise and E. Creusé, *A posteriori error estimation for the heterogeneous Maxwell equations on isotropic and anisotropic meshes*, Calcolo, **40** (2003), pp. 249–271.

22. S. Nicaise, K. Witowski, and B. I. Wohlmuth, *An a posteriori error estimator for the Lamé equation based on equilibrated fluxes*, IMA J. Numer. Anal., **28** (2008), no. 2, pp. 331–353.

23. R. Verfurth, *A review of a posteriori error estimation and adaptive mesh-refinement thecniques*, Teubner Skripten zur Numerik, 1996.